Next Materials 12 (2026) 102095

Contents lists available at ScienceDirect

Next Materials

journal homepage: www.sciencedirect.com/journal/next-materials

Research article

Harnessing *de novo* designed ultrashort self-assembling peptides and silk fibroin as pre-gels for extrusion-based bioprinting

Eugenia Spessot [a], Mohamed A.N. Soliman [b,c], Daniele Campoli [a], Abdulwahhab Khedr [b,d], Gaia Pascolo [a], Antonella Motta [a,e], Devid Maniglio [a], Mohamed A. Elsawy [b,f,*], Annalisa Tirella [a,f,**]

[a] Department of Industrial Engineering, Biotech Research Centre for Biomedical Technologies, University of Trento, Trento, Italy
[b] Leicester School of Pharmacy, De Montfort University, Leicester, UK
[c] Department of Pharmaceutics and Industrial Pharmacy, Faculty of Pharmacy, Cairo University, Cairo, Egypt
[d] Department of Pharmaceutics and Industrial Pharmacy, Faculty of Pharmacy, Zagazig University, Zagazig, Egypt
[e] Department of Biochemistry and Microbiology, Faculty of Pharmaceutical Sciences, Chulalongkorn University, Bangkok, Thailand
[f] Division of Pharmacy and Optometry, University of Manchester, Manchester, UK

ARTICLE INFO

Keywords:
Hydrogels
Silk fibroin
Self-assembling peptides
Extrusion-based bioprinting
Rheology

ABSTRACT

Silk fibroin (SF) hydrogels are widely used in tissue engineering, thanks to its tunable physicochemical properties, aqueous processability and cytocompatibility. However, the use of SF-based inks in extrusion-based bioprinting (EBB) is limited due to SF rheological properties. In this work, we used the de novo designed self-assembling ultrashort ionic-complementary constrained peptides (UICPs) to modulate the rheological profile of SF-based pre-gels. By leveraging the synergistic interaction between SF and UICPs, we successfully modulated the molecular assembly of the pre-gel, significantly enhancing the rheological properties without compromising the integrity of the system. The SF-UICP hybrid formulations were engineered to optimize hydrogelation kinetics and mechanical stability. Furthermore, hyaluronic acid (HA) was incorporated to refine the shear-thinning behavior of the pre-gel, facilitating high-fidelity deposition and reducing the spreading ratio during the extrusion process. Our results demonstrate that UICPs serve as effective enhancers of rheological profiles of SF for EBB. The SF-based biomaterial ink offers an alternative biomaterial for the 3D printing of scaffolds for tissue engineering and regenerative medicine applications.

1. Introduction

Extrusion-based bioprinting (EBB) is an additive manufacturing technique used for the manufacturing of hydrogel-based complex structures for tissue engineering [1–3]. The main challenge related to this technique is the development of biomaterial inks with suitable rheological properties able to guarantee material's extrudability, structural stability of printed objects over time and specific biological outcomes [4–7].

Silk fibroin (SF) is as a promising material for tissue engineering due to its biological properties, ease of functionalization as well as processability in aqueous environments, and tunable mechanical properties [8–11]. However, SF at usual working concentrations (i.e., 2–15% w/v) exhibits unsuitable viscosity and viscoelastic properties for EBB, namely low viscosities and poor shear thinning profile [12,13].

Another shortcoming in using SF-based biomaterial inks for EBB is the hydrogelation mechanism. In fact, physical hydrogels can be formed through the natural conformational transition from random coil to β-sheet of the SF chain, as happens in native spinning, without the need for chemical functionalization of the protein [9,14]. This process can be triggered by environmental stimuli (e.g., temperature, pH level, ionic strength, protein concentration and organic solvents) or via mechanical treatments (e.g., ultrasound exposure and flow-induced shear stresses) [15]. Although these hierarchical molecular assembly mechanisms have been widely exploited in traditional scaffold fabrication (films, sponges, hydrogels) [16], only a few attempts have been reported for the formulation of SF-based biomaterial inks suitable for EBB, mostly requiring the use of coagulation baths or supporting materials to control

* Corresponding author at: Division of Pharmacy and Optometry, University of Manchester, Manchester, UK.
** Corresponding author at: Department of Industrial Engineering, Biotech research centre for biomedical technologies, University of Trento, Trento, Italy.
E-mail addresses: eugenia.spessot@unitn.it (E. Spessot), mohamed.elsawy@manchester.ac.uk (M.A. Elsawy), annalisa.tirella@unitn.it (A. Tirella).

https://doi.org/10.1016/j.nxmate.2026.102095
Received 12 January 2026; Received in revised form 7 April 2026; Accepted 14 April 2026
Available online 21 April 2026

shape fidelity and to tune the gelation kinetics [17]. To exploit the use of SF-based biomaterial inks, other approaches reported in literature attempted the increase of protein concentration up to 20–30% w/v, crosslinking before printing [18], free-form printing [17,19] or blending with other natural-based polymers [20–25] The latter is certainly promising, as the use of polymers with shear thinning profiles (e.g., hyaluronic acid, alginate, pectin) enables facile and precise extrusion and further printing of SF-based biomaterial inks [23,26].

De novo short peptides are interesting molecules able to effectively triggering gelation and form hydrogels from the spontaneous self-assembly into bioinspired supramolecular structures (e.g. β-sheets, β-hairpins, α-helices and coiled coils, and others) through non-covalent interactions, such as hydrogen bonding, electrostatic, π-stacking and hydrophobic interactions [27]. A few recent studies reported the use of peptides as enhancer of rheological profiles of biomaterial inks for EBB [28,29]. Among these, peptides that self-assemble into stable β-sheet nanofibers have gained significant attention due to their ability to form hydrogels in aqueous and physiological environments [30]. In our previous work, we reported on the rationally designed ultrashort ionic-complementary constrained peptides (UICPs), that are capable of self-assembly into thermodynamically stable β-sheet nanofibers which further entangle into mechanically robust supramolecular hydrogels [31]. We have demonstrated the ability of fine-tuning both the nanofiber morphology and the hydrogel rheological properties by the careful molecular design of the amino acid sequence of UICPs, exploiting both aromatic and electrostatic interactions [30,31].

Just recently, small synthetic peptides were used for the first time to trigger SF conformational transition from random coil to β-sheet structure via hydrophobic and hydrogen bonding interactions, thus exploiting a "bottom-up strategy" to produce hybrid hydrogels with tunable properties [32,33]. The use of peptides as additives to SF helped tailoring the biomechanical and bioactive properties of the formed hydrogels; for instance, to improve cell adhesion, due to the lack of RGD-like sequences to the SF primary structure. Moreover, self-assembled peptides showed promising results in formulating biomaterial inks for EBB applications either alone [29,34], or as rheological enhancer for shear thinning materials such as sodium alginate [28] and methylcellulose [35].

In this current study, we have used for the first time β-sheet forming peptides (namely UICP6 and UICP10) to direct the rheological behavior of pristine SF and to formulate new biomaterial inks for EBB. Herein, we show how the formulation of and the interactions within the biomaterial ink drives a successful manufacturing of SF-UICP based three-dimensional (3D) systems. To ensure hydrogel network homogeneity, and further enhance printability tailoring rheological profiles compatible with EBB, hyaluronic acid is included in the biomaterial ink opening for new approaches to be implemented in tissue engineering and regenerative medicine applications.

2. Materials and methods

2.1. Silk fibroin (SF) preparation

Bombyx morii silk cocoons (Chul Thai SilkCo., Phetchabun, Thailand) were first degummed to remove the soluble protein sericin from the silk fibroin fibers adapting a well-known protocol [10]. Briefly, 10 g of cocoons were cut into small pieces and boiled for 30 min in 4 L of 0.02 M sodium carbonate (Na_2CO_3, Sigma-Aldrich) solution and washed three times in DI water for 20 min at room temperature (RT) under stirring. The fibers were then air dried under the fume hood for 48 h. The degummed SF fibers were then dissolved in a 9.3 M LiBr aqueous solution at 65°C for 4 h and dialyzed against deionized (DI) water using Slide-a-Lyzer dialysis cassettes (Spectra/Por Spectrum Laboratories, 3.5 kDa MWCO) for three days at RT to remove the excess of LiBr (aq.). SF solution was centrifuged twice at 9000 rpm at + 4 °C for 20 min to remove the impurities, concentrated in air for approximately 10 h upon reaching the concentration of 7% w/v and then stored at + 4 °C and used within 7 days. The concentration of the solution was measured by checking the intensity of the peak at 280 nm by UV spectroscopy (Nanodrop 1000, ThermoFisher Scientific, Waltham, MA, USA).

2.2. Self-assembled hydrogel preparation

2.2.1. Peptides selection and peptide-based pre-gel preparation

Two peptides, Table 1, (Biomatik USA, LLC, purity >95%) were selected to study the influence of the peptide charge on the SF self-assembly and their interactions.

The selected peptides shared a similar self-assembly mechanism [30]. The charge was calculated with Eq. 1:

$$z = \sum_i N_i \frac{10^{pKa_i}}{10^{pH}+10^{pKa_i}} - \sum_j N_j \frac{10^{pH}}{10^{pH}+10^{pKaj}} \quad (1)$$

$N_{i/j}$ represents the numbers while $pKa_{i/j}$ refers to the pKa values of the basic (i - pKa > 7) and acidic (j - pKa < 7) groups in peptide.

The peptide-based hydrogels were prepared as previously described in Wychowaniec et al. Wychowaniec et al. [31]. Briefly, peptide powders were dissolved in HPLC water by vortexing at 2500 rpm at RT. To trigger the gelation, the pH of the peptide solution was adjusted to 4.5–5.0 by stepwise addition of 0.5 M NaOH solution (aq.), followed by vortexing for 30–60 s between each addition, and being this the final pH of pre-gels. Then, the final volume was adjusted by adding HPLC water to obtain the target final concentrations (all tested conditions are reported in Table 2). The as-prepared hydrogels were left at + 4 °C for 24 h. The Critical Gelation Concentration (CGC) was assessed via inversion vial test by monitoring the minimum peptide concentration necessary to have the formation of a gel-like structure without gravitational flow as described in our previous works [30,31].

2.2.2. Standard mixing protocol for SF-UICP pre-gel preparation

For the preparation of the SF-UICP pre-gels, the peptide powder was dissolved in HPLC water (two thirds of the final volume), and the pH was adjusted at 3.5 by stepwise addition of 0.5 M NaOH (aq.). Then, the SF solution was added in a 1:1 vol ratio to the peptide aqueous phase and homogenized by gentle stirring. The pH was adjusted at 4.5–5.0 by stepwise addition of 0.5 M NaOH solution to trigger the peptide gelation. Final volume was adjusted with HPLC water to obtain the required concentrations (Tables 3 and 4). Hydrogels were equilibrated at + 4 °C for 24 h and characterized via inversion vial test for the detection of the CGC and further physico-chemical characterization.

Only when explicitly reported, a 2.0% w/v of methacrylated hyaluronic acid (HAMA) aqueous solution was added to the SF-UICP solution for printability studies (Table 5). The hyaluronic acid (HA, 1.0–1.5 MDa, Glentham Life Sciences) methacrylation reaction was performed as reported by Loebel et al. [36].

2.3. Characterization of the self-assembled pre-gels

2.3.1. Thioflavin T fluorescence assay (ThT)

The Thioflavin T (ThT) is a fluorescent dye that binds to amyloid-like β-sheet fibrils structures, and the ThT assay allows to monitor the self-assembly kinetics *in vitro* [37]. ThT assay was used in this study to detect the β-sheet formation under the different conditions. A 1 mM ThT stock solution was prepared in HPLC water and then added to the peptide aqueous phase with a final concentration of 100 μM before

Table 1
Tested peptides and properties, including name, sequence, molecular mass and net charge at pH 4.5–5.0.

Peptide name (Code)	Peptide sequence	Net Charge at pH = 4.5–5.0
UICP6 (P)	Phg-Lys-Phg-Glu	0
UICP10 (E)	Glu-Phg-Lys-Phg-Glu	-1

Table 2
Tested peptide-based formulations to assess the critical gelation concentration.

Peptide name (Code)	Peptide final concentration [% w/v]	Label
UICP6 (P)	0.5	P0.5
	1.0	P1
	2.0	P2
	3.0	P3
	4.0	P4
	5.0	P5
	6.0	P6
UICP10 (E)	0.5	E0.5
	1.0	E1
	2.0	E2
	3.0	E3
	4.0	E4
	5.0	E5

Table 3
SF-E biomaterial ink formulations tested to assess hydrogelation.

Silk Fibroin [% w/v]	UICP10 (E) [% w/v]	Code
3.0	2.0	SF3-E2
	3.0	SF3-E3
	4.0	SF3-E4
	5.0	SF3-E5

Table 4
SF-P biomaterial ink formulations tested to assess hydrogelation. Of note, the concentration of P peptide tested is within the self-assembly concentration range (Fig. 1D).

Silk Fibroin [% w/v]	UICP6 (P) [% w/v]	Code
2.0	2.0	SF2-P2
	3.0	SF2-P3
	4.0	SF2-P4
	5.0	SF2-P5
2.5	2.0	SF2.5-P2
	3.0	SF2.5-P3
	4.0	SF2.5-P4
	5.0	SF2.5-P5
3.0	2.0	SF3-P2
	3.0	SF3-P3
	4.0	SF3-P4
	5.0	SF3-P5
3.5	2.0	SF3.5-P2
	3.0	SF3.5-P3
	4.0	SF3.5-P4
	5.0	SF3.5-P5

Table 5
Biomaterial ink formulations tested to assess printability.

Silk Fibroin [% w/v]	UICP6 (P) [% w/v]	HAMA [% w/v]	LAP [% w/v]	Code
3.5	-	2.0	0.5	SF3.5-H2
3.5	4.0	2.0	0.5	SF3.5-P4-H2
-	-	2.0	0.5	H2

proceeding. A SpectraMax M5 spectrofluorometer plate reader (excitation wavelength 440 nm, cutoff wavelength 475 nm, emission wavelength 490 nm) was used to measure the fluorescence (scan range 460–600 nm) after 30 min, 1 h, 2 h, 4 h, 6 h, 8 h, 24 h, 48 h, 72 h and 96 h. All conditions were performed in triplicates.

2.3.2. Attenuated total reflectance Fourier-transform Infrared Spectroscopy (ATR-FTIR)

The secondary structure of the self-assembled pre-gels was determined by Fourier Transform Infrared Spectroscopy (FT-IR) using a Thermo Nicolet IR200 spectrophotometer equipped with a diamond multibounce attenuated total reflectance (ATR) plate. Transmittance measurements were carried out from 4000 to 400 cm^{-1} at 128 scans and a resolution of 2 cm^{-1} using HPLC water as the background. All spectra were subtracted automatically from the background by OPUS software version 8.1. Peak deconvolution for the amide I bands from 1600 to 1700 cm^{-1} was then performed via OriginPro™ 2016 software to separate peaks and determine the peak areas. β-sheet content was estimated per sample by calculating the percentage of the deconvoluted peak area for the peak at 1620–1625 cm^{-1} in relation to the overall area of the amide I band.

2.3.3. Rheological characterization

Rheological evaluations were performed on a Discovery Hybrid Rheometer HR-2 rheometer (TA Instruments, The Netherlands) equipped with a 25 mm parallel plate geometry and a Peltier plate for the temperature control. A closed chamber was used to minimize solvent evaporation. To investigate the flow behavior of the solutions, rotational shear rate sweeps (0.1–50 s^{-1}) have been carried out to analyze the viscosity profile. An oscillatory stress sweep test (0.1–1000 Pa, 1 Hz) was performed to determine the viscoelastic properties of the material: storage (G'), loss (G'') moduli, and loss factor (tanδ) were evaluated by averaging the points (n = 10) in the LVER.

2.3.4. Morphological characterization: scanning electron microscopy (SEM)

Scanning electron microscopy (SEM, Carl Zeiss EVO LS 15) was used to investigate the inner morphology of SF-UICP pre-gels. The UICP and the SF-UICP pre-gels were deposited on an aluminum stub with a carbon tab, freeze-dried and gold sputter-coated before imaging.

2.3.5. Printability tests

Biomaterial inks were printed using a BIO X™ (CELLINK, Boston, USA) extrusion-based bioprinter (EBB) equipped with pneumatic printheads. Briefly, the solutions were loaded into a 3 mL cartridge equipped with a 25 G polypropylene conical nozzle (length 32 mm, diameter 0.25 mm) and printed on a Petri dish. Tests were performed following our previous study [38]. The extrudability of the pre-gelled biomaterial inks and the filament formation capability was evaluated by slowly increasing the printing pressure until the biomaterial ink started to extrude steadily, hence identifying the minimum extrusion pressure defined as the minimum pressure allowing the extrusion of a continuous and homogeneous filament from the nozzle. Straight line geometries (5 strands of 3 cm length) were printed for each composition at three different extrusion velocities and at three extrusion pressures to optimize the printing parameters. Two quantitative parameters were considered for the analysis of the shape fidelity: the Spreading Ratio (SR) and the Uniformity Factor (UF), being respectively the ratio between the width of the extruded strand over the printing needle diameter (250 μm) and the ratio between the length of the extruded strand and the length of the theoretical straight strand.

2.4. Characterization of the printed hydrogels

2.4.1. Stability tests

The stability of the printable formulations was tested on hydrogels immersed in phosphate buffered solution (PBS, Sigma-Aldrich P3816) by monitoring their weight variation over time. Briefly, 500 μL of material with 0.5% w/v of LAP were extruded in silicon molds (n = 3) and exposed for 1 min to a 405 nm lamp. The obtained cylinders were weighed as prepared (W_0) and immersed in 2 mL of PBS, then incubated at 37 °C. At each timepoint (30 min, 1 h, 2 h, 4 h, 8 h, 24 h, 48 h, 72 h, 7 d, 14 d), samples were removed from the buffer, excess water was absorbed with filter paper, and samples were weighted (W_1). The swelling ratio was calculated as in [39] with the Eq. 2:

Swelling Ratio (%)= (W1 − W0)/W0 (2)

2.4.2. Morphological analysis

Field emission Scanning electron microscopy (FE-SEM, Carl Zeiss Supra 40) was used to investigate the inner morphology of extruded and photocrosslinked hydrogels. The hydrogels were prepared as described in 2.4.1, freeze-dried and Pt/Pd sputter-coated before imaging.

2.5. Statistical analysis

The statistical analysis of the data was performed using a two-way analysis of variance (ANOVA) using OriginPRO v2018. Bonferroni's multiple comparison test was used to evaluate significant differences among the tested conditions. p-values were set at four levels having $p \leq 0.05$ and indicated in the figures as * $p \leq 0.05$, ** $p \leq 0.01$, *** $p \leq 0.001$, **** $p \leq 0.0001$, ns > 0.05.

3. Results and discussion

3.1. Peptide-based pre-gels: selection and preliminary characterization

The molecular, physicochemical and mechanical properties of the two peptides (Table 1) used for this study, i.e. UICP6 (referred to as P) and UICP10 (referred to as E), were previously fully characterized in our published work [30].

The two peptides were re-characterized for their self-assembly and hydrogelation ability also in the current study for a comparison with the SF-UICP pre-gels. The molecular design of the selected peptides was bioinspired from a segment of the yeast nuclear protein Zuotin, where the short sequence possesses alternating charges (either Lys or Glu) and aromatic phenylglycine residues. This ionic self-complementary sequence pattern allowed self-assembly into stable antiparallel β-sheet fibrils [30,31,40]. These peptides, above a critical gelation concentration (CGC), can entangle and interact to form three-dimensional (3D) networks with the ability of retaining water, thus forming self-supportive hydrogels.

The chosen UICPs have different theoretical net charges (Z) at the gelation pH 4.5–5.0, which is calculated as Z = 0 (i.e. neutral) for UICP6 and Z = -1 (i.e. anionic) for UICP10 (Fig. 1A and Table 1). The gelation pH of both peptides is slightly above the isoelectric point of SF (pI = 3.8–3.9) [41], ensuring that the protein net charge is neutral to negative, hence avoiding SF precipitation. In addition, both peptides exhibited the highest β-sheet content at pH 4.5–5, which is expected to enhance the UICP-SF co-assembly through β-sheet nucleation [30]. Cationic UICPs were not used to avoid charge driven SF-UICP aggregating that could lead to precipitation. A series of UICP6 and UICP10 concentrations were prepared and screened for their ability to form stable hydrogels at the concentration range 0.5–6.0% w/v at the same pH value (Table 2). For ease reference to their concentration, from now on UICP6 and UICP10 are named P and E, respectively, and followed by a number indicating their concentration (% w/v), as shown in Table 2. The CGC was estimated through the inversion vial test, which was shown to be 3.0% w/v and 2.0% w/v for P and E, respectively, and consistent with our previous study (Fig. 1B) [30]. An increased opacity was observed as a function of hydrogel concentration for both P and E peptides (Fig. 1B). This behavior is a result of entanglement and further aggregation of β-sheet bundles at higher hydrogel concentrations causing scattering of light [42]. Scanning electron microscopy (SEM) micrographs of both P4 (Fig. 1C) and E5 (Fig. 1E) confirmed the ability of the two peptides to form an organized structure at the CGC, with an internal microstructure displaying an irregular filamentous porous network. The similarity of the two morphologies was related to the shared self-assembly mechanism [30].

Molecular characterization of self-assembly was performed using ATR-FTIR analysis. The FTIR spectra of different P peptide concentrations revealed a characteristic β-sheet peak at 1620 cm^{-1} with a random

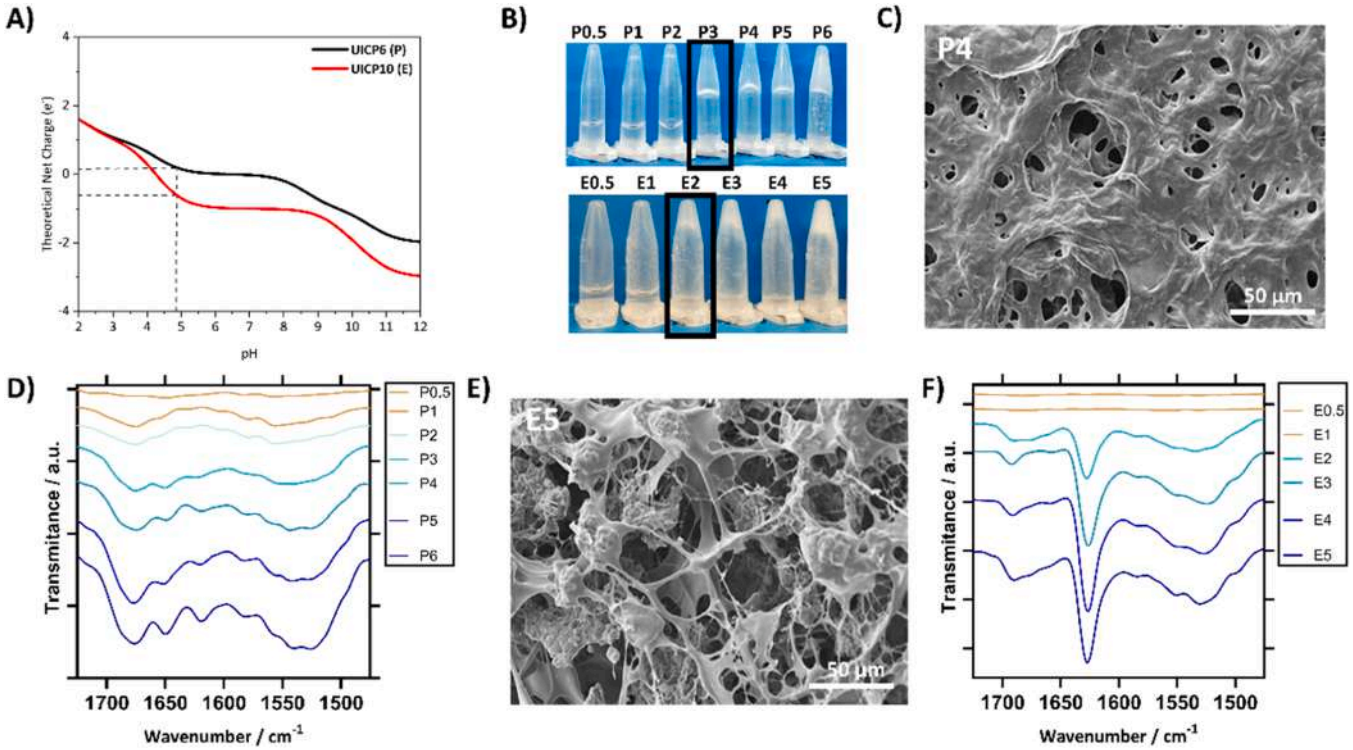

Fig. 1. Characterization of UICP6 (P) and UICP10 (E) peptides: A) theoretical net charge, B) inverted vial tests (CGC framed in black), C) SEM micrograph of P4 (Scale bar = 50 μm), D) ATR-FTIR spectra showing amide I band of P peptide samples at concentration range of 0.5–5% W/V, E) SEM micrograph of E5 (Scale bar = 50 μm), F) ATR-FTIR spectra showing amide I band of E samples in concentration range of 0.5–5% w/v.

coil peak at 1647 cm^{-1} at concentrations of 3.0–6.0% w/v (P3-P6, Fig. 1D), while for the E peptide a sharp β-sheet peak (1625 cm^{-1}) in the amide I region was observed at concentrations of 2.0–5.0% w/v (E2-E5, Fig. 1F). A broad peak at 1525 cm^{-1} was also observed in amide II band, indicating an extended β-sheet structure. These findings are in agreement with our recent study by Soliman et al. [30]. The higher β-sheet content observed with the E peptide is attributed to the difference in the net charge between P and E peptides (Fig. 1A), suggesting that neutral P peptide may be a more suitable candidate for interaction with SF. To investigate this hypothesis, both P and E peptides were subsequently formulated with SF in different combinations.

3.2. Self-assembled SF-UICP pre-gels: preliminary screening

Following characterization of P and E peptides, their interaction with SF was studied as hydrogelation promotor and rheological enhancer additives. Concentration ranges identified (Fig. 1) were selected for the formulation of SF-UICP biomaterial inks for EBB.

First, the interaction of different concentrations of the anionic E peptide (concentration range 2.0–5.0% w/v, Fig. 1F) with a 3.0% w/v SF was explored, using the SF-E biomaterial inks detailed in Table 3.

From the inversion vial test, it was possible to confirm that all the tested SF-E samples have successfully formed hydrogels, thus confirming the suitability of the E peptide in facilitating the hydrogelation of 3.0% w/v SF starting from a concentration of 2.0% w/v (Fig. 2). Of note and as expected, pristine SF used as control failed to form hydrogel at pH 4.5, which is well above the isoelectric point of the protein (pH = 3.8 – 3.9) [41].

However, after stirring to check the homogeneity of the gel, all SF-E3 hydrogel displayed phase separation among the self-assembled material (white gummy-like phase) and the water phase (transparent), as shown in Fig. 2 insert. This behavior under the presence of external physical stress could cause hydrogel syneresis [43]. Due to the observed instability, the SF-E biomaterial inks did not show suitable behavior for its extrusion and further use for EBB.

We then tested the interaction of the neutral P peptide varying SF concentrations (i.e., 2.0–3.5% w/v), limiting its concentrations in the range of 2.0–5.0% w/v for ease comparison with E peptide, as reported in Table 4.

Unlike SF-E pre-gels, a concentration dependent behavior between P and SF was observed for all SF-P formulations (Fig. 3, inverted vial tests). Whilst pristine SF and SF-P2 failed to form hydrogels as observed from the inverted vial test (regardless of SF concentration); successful hydrogelation of SF-P mixtures was achieved at P peptide concentrations equivalent to or higher than the CGC value (i.e., $\geq$ 3.0% w/v, Fig. 3). The SF-P pre-gels had a translucent appearance, enhanced with the increase of P concentration in the system (Fig. 3). Such visual difference in the hydrogels suggests structural re-organization of the fibrils of both SF and P in the hydrogel network, which could have possibly resulted in a homogeneous SF-P hybrid system.

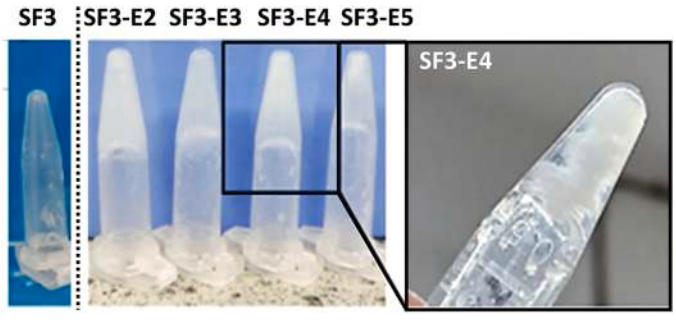

Fig. 2. Assessment of SF-E hydrogelation behavior: Inverted vial test on SF3-E formulations (on the left) and phase separation after shear (on the right). The insert shows the details of phase separation after gentle stirring of SF3-E4 hydrogel, selected as example.

Based on these hydrogelation studies, only the SF-P pre-gels were used throughout the rest of this study to investigate its printability, whilst the SF-E pre-gel was excluded due to the high potential of physical instability under external forces (e.g., flow-induced shear stresses).

3.3. Self-assembled SF-P system: hydrogelation mechanism and kinetics

To further understand the interaction between SF and P, molecular secondary structure and nanoscopic morphology of the SF-P pre-gels were studied using ATR-FTIR spectroscopy and SEM, respectively. In addition, hydrogelation kinetics was evaluated via quantifying β-sheet nanofiber formation using Thioflavin T (ThT) binding fluorescence spectroscopy [37]. As SF-P hydrogelation was found to be concentration dependent (Fig. 3), we then focused on the study of SF-P pre-gels using the highest concentrations of SF (i.e., 3.0 and 3.5% w/v), with the aim of maximizing the SF content in the biomaterial ink.

The ATR-FTIR spectra of both pristine SF and SF-P pre-gels presented distinct prominent peaks at amide I region (C═O stretching; 1700–1600 cm^{-1}) and at 1545 cm^{-1} assigned to the amide II region (C-N stretching and N-H bending) (Fig. 4) [44]. The peak at 1250 cm^{-1} mainly present in SF samples was assigned to amide III region (C-N stretching and N-H bending) [45].

To further understand the effect of P peptide on the SF structure, amide I band peak deconvolution was performed to analyze the SF-P pre-gels secondary structure (Fig. 5). Pristine SF3 was mainly unstructured (~61% random coil) with minor 18% β-sheet population (Fig. 5A). Interestingly, addition of P3 (i.e. SF3-P3) led to a 2-fold increase in β-sheet structure (~36%) and a significant reduction in unstructured population (~31% random coil) (Fig. 5B). Further increase in the peptide concentration within the mixture (i.e. SF3-P4) only led to a slight increase in β-sheet population (~40%) (Fig. 5C), with no further change observed for SF3-P5 structure (*data not shown*). Likewise, the SF3.5 based formulations showed a similar secondary structure profiles, with a significant increase in β-sheet population (~32%) with the addition of P3 (i.e. SF3.5-P3) (*data not shown*).

The morphology of SF3-P4, SF3.5-P4, SF3-P5 and SF3.5-P5 samples was further characterized by investigating SEM micrographs to confirm the supramolecular assembly into nanofibers and formation of entangled networks. All tested SF-P pre-gels showed a highly interconnected porous structure (Fig. 6) similar to that observed for P4 self-assembled hydrogels (Fig. 1C). The mean diameter of the pores for all the tested formulations was in the range 10–50 μm, considered acceptable for promoting a biological outcome in future experiments [46].

Evaluation of the rate and extent of β-sheet nanofiber formation in SF-P pre-gels, via ThT binding fluorescence assay, also revealed a peptide concentration dependency (Fig. 7). Strikingly, the β-sheet nanofiber formation level of the individual mixture components (i.e., pristine SF3 and SF3.5, and the pure peptide samples P4 and P5), was lower than that of the SF-P systems with significantly lower formation kinetics, implying co-assembly through β-sheet nucleation (Figs. 7A and 7B), aligning well with the molecular characterization of secondary structures (Fig. 5) and the natural assembly process occurring in SF after its regeneration [47]. Blending SF with P led the system to a faster hydrogelation kinetics with a correlation with both P and SF concentrations. Of note, a higher fluorescence intensity (Fig. 7) corresponds to a higher SF concentration in the system; nevertheless, a correlation with P concentration is detected, confirming the dependence of P concentration in SF-P pre-gels and consequent formation of β-sheet secondary structures (as shown in Fig. 5).

Based on the above results, a hypothesis on the interaction mechanism between SF and P was postulated. SF hydrogelation usually occurs with a nucleation and growth process in which SF chains form β-crystallites first, which evolve into β-crystallites networks (nanofibrils) [48–50]. Nanofibrils growth and branching into single-domain fibril then occur, which interpenetrate forming multidomain fibril network

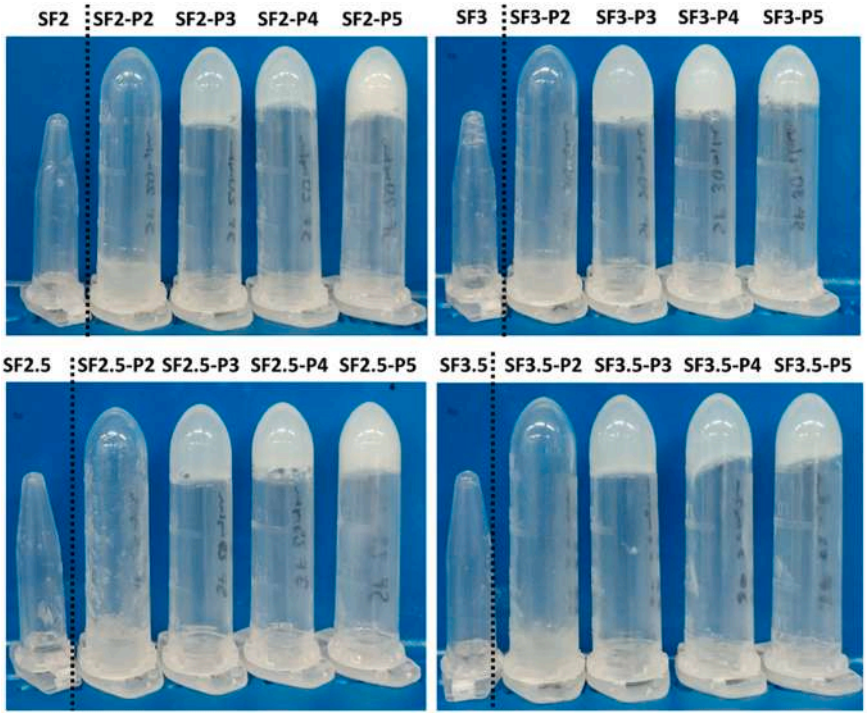

Fig. 3. Inverted vial test for SF-P mixtures: visual assessment of SF-P hydrogelation using different concentrations of SF and P peptide.

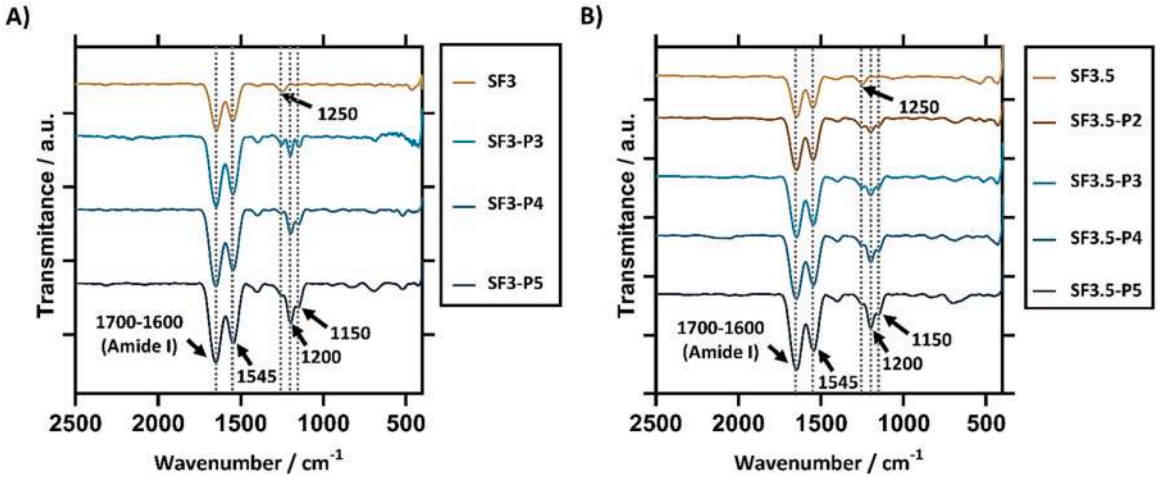

Fig. 4. ATR- FTIR spectra of A) SF3-P and B) SF3.5-P pre-gels.

with weak intra-domain interactions. With time, the domains stabilize to form hydrogel networks, if the Gibbs free-energy barrier is overcome [51].

In this study, the molecular secondary structure profiles and the nanofibers formation kinetics of the SF-P systems suggest a nucleation-mediated co-assembly mechanism. The P fibrils offered heterogeneous nucleation sites for the β-sheet fibrils domains of SF, thus explaining the faster hydrogelation kinetics and the higher β-sheet content compared to pristine SF (Fig. 8). The continuous increase in the ThT fluorescence of SF-P systems up to 96 h suggested that 24 h was not the late-stage of β-sheet crystallites formation, thus supporting the coexistence of random coil and β-sheet structures (Fig. 7C). This confirmed the suitability of P for its use as pre-crosslinker for SF in the design of a biomaterial ink for EBB.

3.4. Rheology of SF-P hydrogels

To further investigate the suitability of SF-P pre-gels as biomaterial inks for EBB, rheological tests were performed. As previously discussed, the main challenge of using SF in EBB is the poor viscosity and visco-elasticity. Previous tests show that the inclusion of P in SF solutions promotes formation of β-sheet compared to pristine SF (Figs. 4, 5 and 7). To further confirm the role of P as rheological enhancer of SF by inducing a pre-crosslinking (i.e., a partial hydrogelation of the solution), different tests were performed to meet the biomaterial inks attribute requirements for the extrusion process.

Generally, a shear thinning behavior is required to enable the solution to flow through the printing needle when an extrusion pressure is applied. Moreover, a viscosity in the range $1–6 \times 10^4$ Pa·s [52] is requested for processing polymeric aqueous solutions with EBB without the need of using a supporting material [19]. Flow sweep tests were

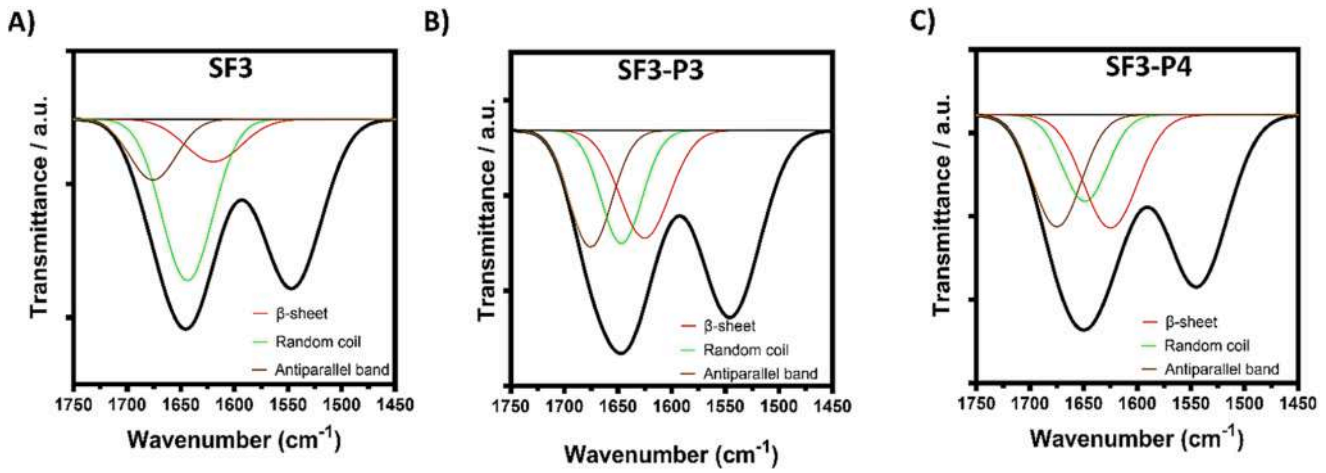

SF3			
Structure	β-sheet	Random coil	Antiparallel band
Position (cm^{-1})	1620	1644	1675
Area	42.29	143.22	49.32
Ass/Amide I (%)	18.01	60.99	21.00

SF3-P3			
Structure	β-sheet	Random coil	Antiparallel band
Position (cm^{-1})	1625	1647	1675
Area	130.89	113.04	120.86
Ass/Amide I (%)	35.88	30.99	33.13

SF3-P4			
Structure	β-sheet	Random coil	Antiparallel band
Position (cm^{-1})	1625	1649	1675
Area	170.64	107.15	150.48
Ass/Amide I (%)	39.84	25.02	35.14

Fig. 5. Deconvolution of the amide I band for the A) SF3, B) SF3-P3 and C) SF3-P4 ATR- FTIR spectra. The % of secondary structure populations (Ass/Amide I) are presented in the tables at the bottom panel, as the percentage ratio of the relevant C═O stretching peak area (Ass) to the total amide I band peaks area (Amide I).

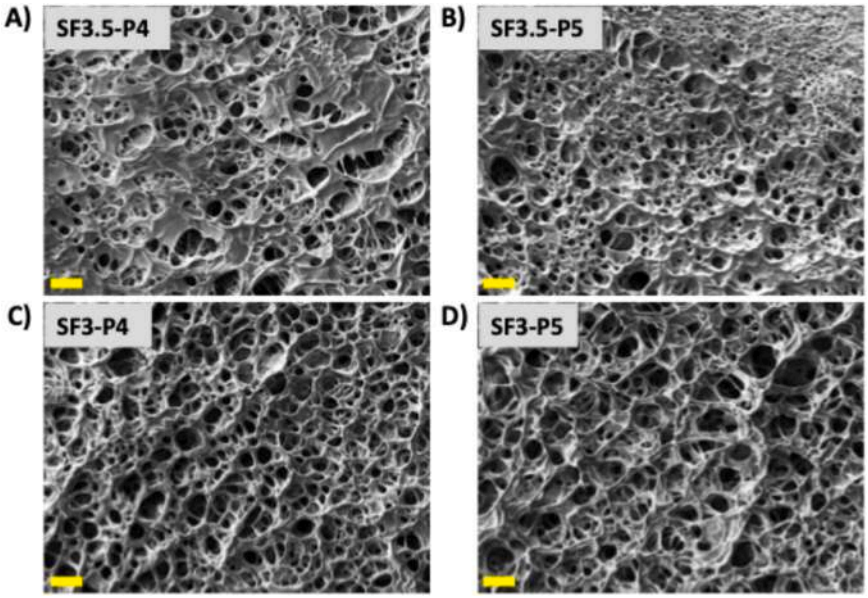

Fig. 6. Scanning electron microscopy (SEM) micrographs showing the morphological features of A) SF3.5-P4, B) SF3.5-P5, C) SF3-P4 and D) SF3-P5 hydrogels (Scale bars = 50 μm).

performed to test the viscosity profile of the pristine SF and SF-P pre-gels (Fig. 9A). All the SF-P samples exhibited a decrease in viscosity with the increase in the shear rate, thus confirming the non-Newtonian nature of the materials, an essential feature to ensure printability. Of note, the viscosity profile of SF3.5 demonstrated low viscosity values (0.01–0.1 Pa·s) with a mild shear thinning behavior confirming the unsuitability of using pristine SF as biomaterial ink for EBB.

From rotational shear rate sweeps, it was possible to notice that SF3.5-P4 and SF3.5-P5 pre-gels displayed the highest viscosities when compared to the equivalents SF3-P4 and SF3-P5 (Fig. 9A), as expected and confirming the influence of SF concentration to match the range of viscosities required for EBB [53]. It is worth noting that all the tests were performed using shear rates in the range of 0.1–50 s^{-1} and avoiding the use of higher shear rates to limit the phenomenon of edge fracture, as reported in our previous work [38] and in literature [54,55].

Further, rheological tests were performed to determine the viscoelasticity of the SF-P pre-gels under oscillatory stresses evaluating the storage (G') and loss (G'') moduli (Fig. 9B), which are usually correlated to filament formation in EBB and shape retention after deposition on the printing bed [7,38,56]. All SF-P pre-gels displayed G' values with an order of magnitude higher than G'' in the linear viscoelastic region (LVER), confirming an elastic-dominated rheological behavior, previously observed in the inverted vial tests (Fig. 3). Differently from SF-P pre-gels, pristine SF (SF3.5, Fig. 9B) had G'' values higher than G' values confirming a liquid-like behavior.

Of note, the highest increase in both G' and G'' values was observed

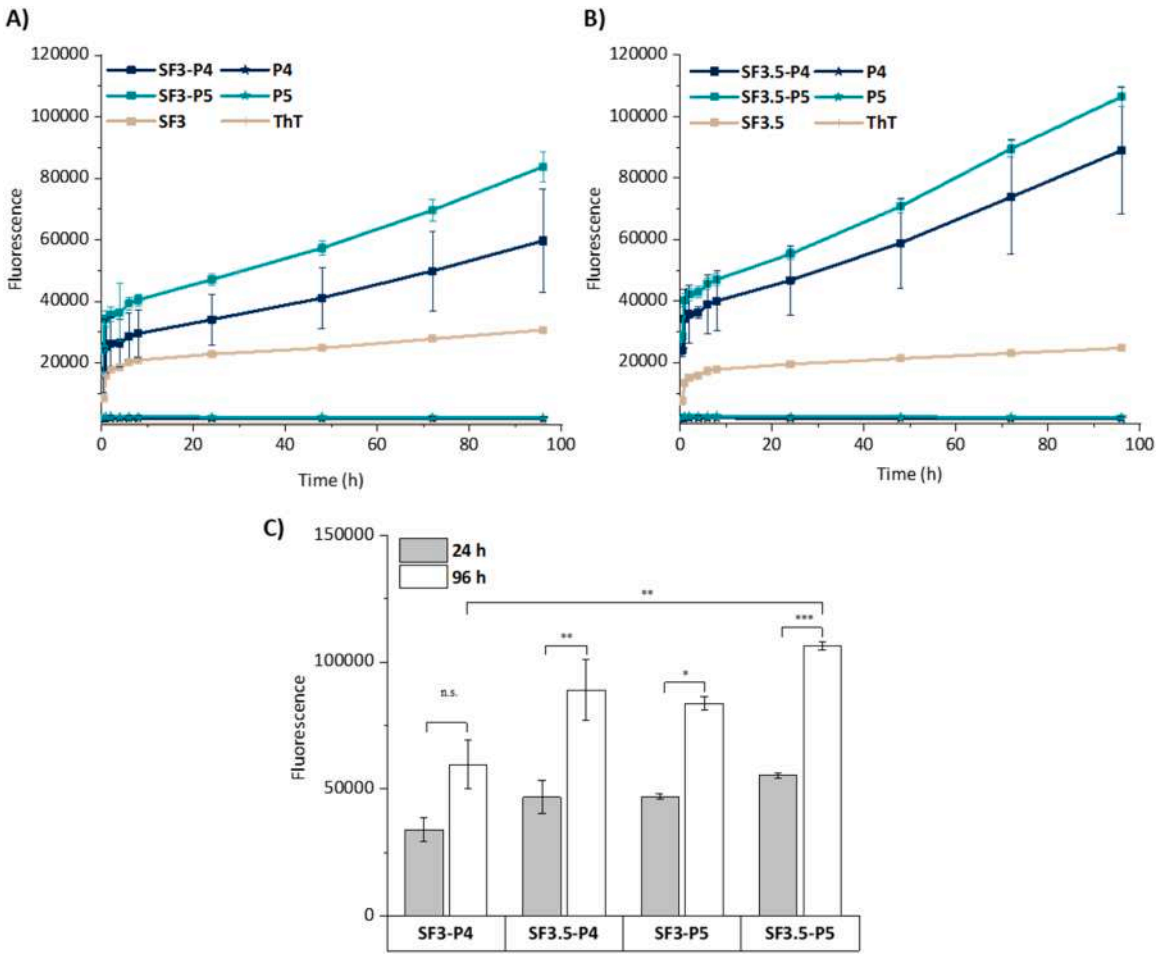

Fig. 7. Kinetics of self-assembly up until 96 h: Thioflavin T assay curves of A) SF3-P and B) SF3.5-P. C) Comparison of fluorescence intensity (mean ± SD) of SF3-P4, SF3.5-P4, SF3-P5 and SF3.5-P5 pre-gels at selected timepoints (i.e., 24 h and 96 h). * $p \leq 0.05$, ** $p \leq 0.01$, *** $p \leq 0.001$, ns > 0.05.

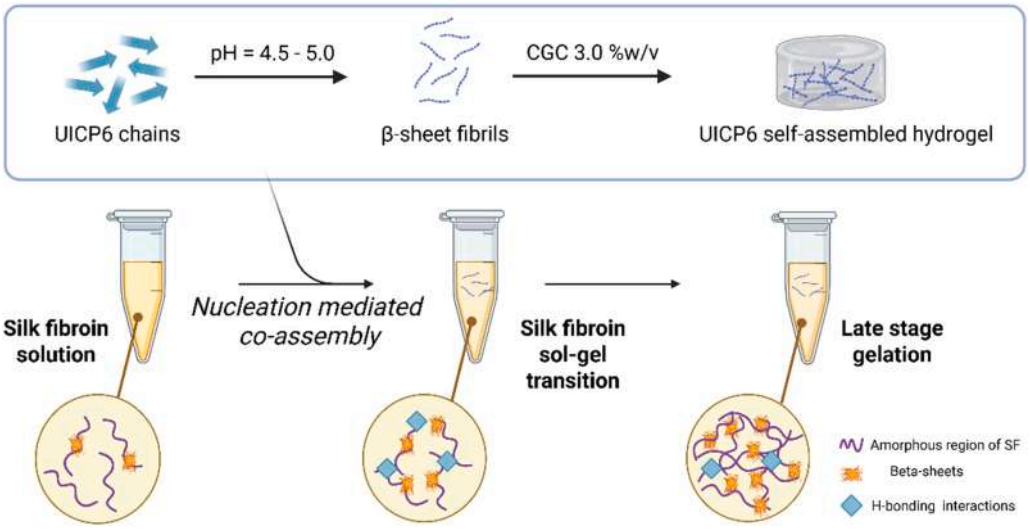

Fig. 8. Proposed schematics of the mechanism of interaction and gelation between SF and P. Created with BioRender.com.

with 3.5% w/v SF concentrations (Fig. 9C). As expected, the SF concentration in the SF-P pre-gels enhanced the hydrogels mechanical stiffness: 376 ± 16 Pa (SF3-P4) vs 1254 ± 121 Pa (SF3.5-P4) and 649 ± 21 Pa (SF3-P5) vs 2208 ± 62 Pa (SF3.5-P5). The higher G' values of SF3.5-P4 and SF3.5-P5 pre-gels suggest a higher interaction among the polymeric chains resulting in higher crosslinking degree with more β-sheet nanofibers, in accordance with ThT binding fluorescence data (Fig. 7). Interestingly, an increase in P concentration from 4.0% w/v to 5.0% w/v doubled the G' value of SF-P pre-gels.

Finally, all the tested SF-P samples showed both a yield (i.e., the limit

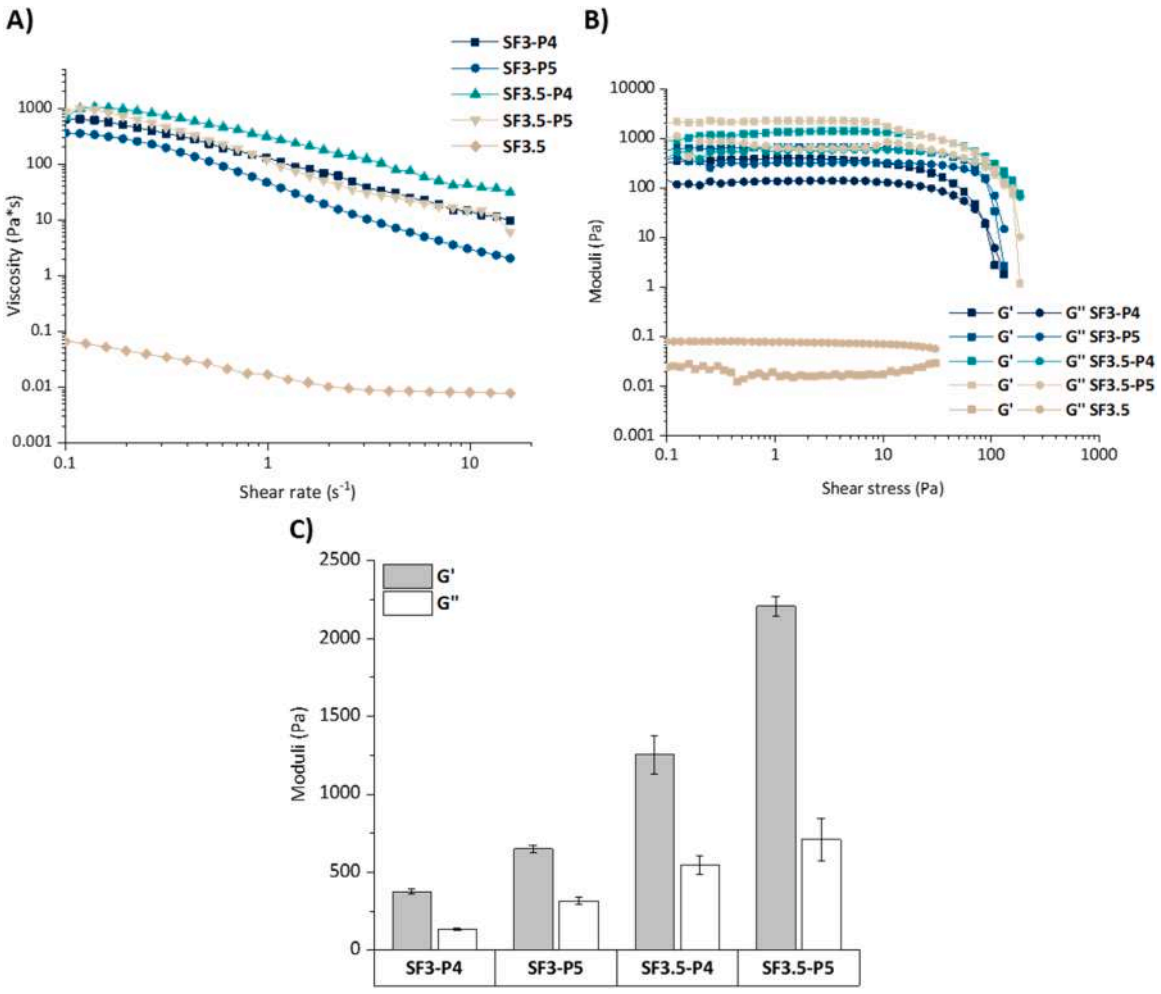

Fig. 9. Rheological tests on SF-P pre-gels. A) Flow sweep curves, B) Oscillation stress curves and C) G' and G'' values (mean ± SD) in the LVER.

of the LVER) and a flow (i.e., the intersection point of G'' and G' curves) points (Fig. 9). These values, together with the loss factor (tan δ) values, predict suitability of SF-P biomaterial inks for EBB. In the materials herein tested, tan δ is within 0.35–0.5 in the LVER, that is well in accordance with the current state of the art for EBB that identifies and optimal tan δ range of 0.25–0.60 for printability [5,57,58].

3.5. Printability tests

Due to the favorable rheological properties, along with its lower peptide content and higher SF content, SF3.5-P4 was selected as a candidate biomaterial ink for EBB studies. A preliminary extrudability test was performed following the protocol previously reported in [59]. Despite its promising rheological properties, SF3.5-P4 pre-gel could only be extruded through a 25 G conical needle and using a minimum extrusion pressure of 30 kPa showing a non-homogeneous and discontinuous filament. Phase separation of liquid and gel phases was observed during extrusion, with an appearance similar to that observed for SF-E hydrogels (Fig. 2). This behavior is likely attributed to hydrogel syneresis happening during extrusion and due to shear stresses within the printing nozzle, which could exceed the weak non-covalent interactions within the SF-P nucleation-mediated co-assembled system (enhanced by the presence of both shear and extensional flow in the syringe) [60,61]. To address this issue, it was decided to include a highly hydrophilic viscous component with known shear thinning properties to the SF-P pre-gel with the hypothesis to obtain a smooth and continuous filament. In specific, we selected the hyaluronic acid methacrylate (HAMA) [62] thanks to its exceptional hydrophilicity and with the scope to retain the liquid phase and prevent SF-P syneresis during extrusion. HAMA concentration was optimized to obtain printable SF-based biomaterial ink (*data not shown*), and identifying the most suitable concentration of 2.0% w/v HAMA. We further used the final composition of the biomaterial ink for EBB as SF3.5-P4-H2. Of note, SF3.5-H2 and SF3.5-P4 biomaterial inks were selected as controls.

Results of the rheological testing confirmed the shear-thinning behavior of the SF3.5-P4-H2 ink to be almost identical to that of SF3.5-P4, both with higher viscosity values when compared to SF3.5-H2 (Fig. 10A). These results confirm that the use of the peptide is beneficial also in presence of a highly hydrated and shear thinning polymer, such as HAMA, with viscosities of pre-gels being SF3.5-P4 ≥ SF3.5-P4-H2 > SF3.5-H2. Moreover, the viscoelastic profiles show a similar trend, with SF3.5-P4-H2 with G' values (~ 302 ± 10 Pa) higher than SF3.5-H2 and lower than SF3.5-P4.

This trend is also displayed by the tan δ in the LVER with an increase from approx. 0.45 for SF3.5-P4 to approx. 0.48 for SF3.5-P4-H2. The higher tan δ value of SF3.5-H2 is approx. 0.57, confirming the presence of a highly hydrated viscous component (i.e., HAMA) in the blend SF3.5-H2 and the lack of a pre-gelation of the biomaterial ink in terms of self-assembling in the presence of the peptide. Importantly, the extent of the SF3.5-P4-H2 LVER increases in comparison with the one of SF3.5-P4, implying enhancement of elasticity and structural integrity of the pre-gel (Fig. 10B) promising for its use as biomaterial ink.

Additionally, all the tested samples (SF3.5-P4, SF3.5-H2 and SF3.5-P4) were able to recover their storage modulus G' after the

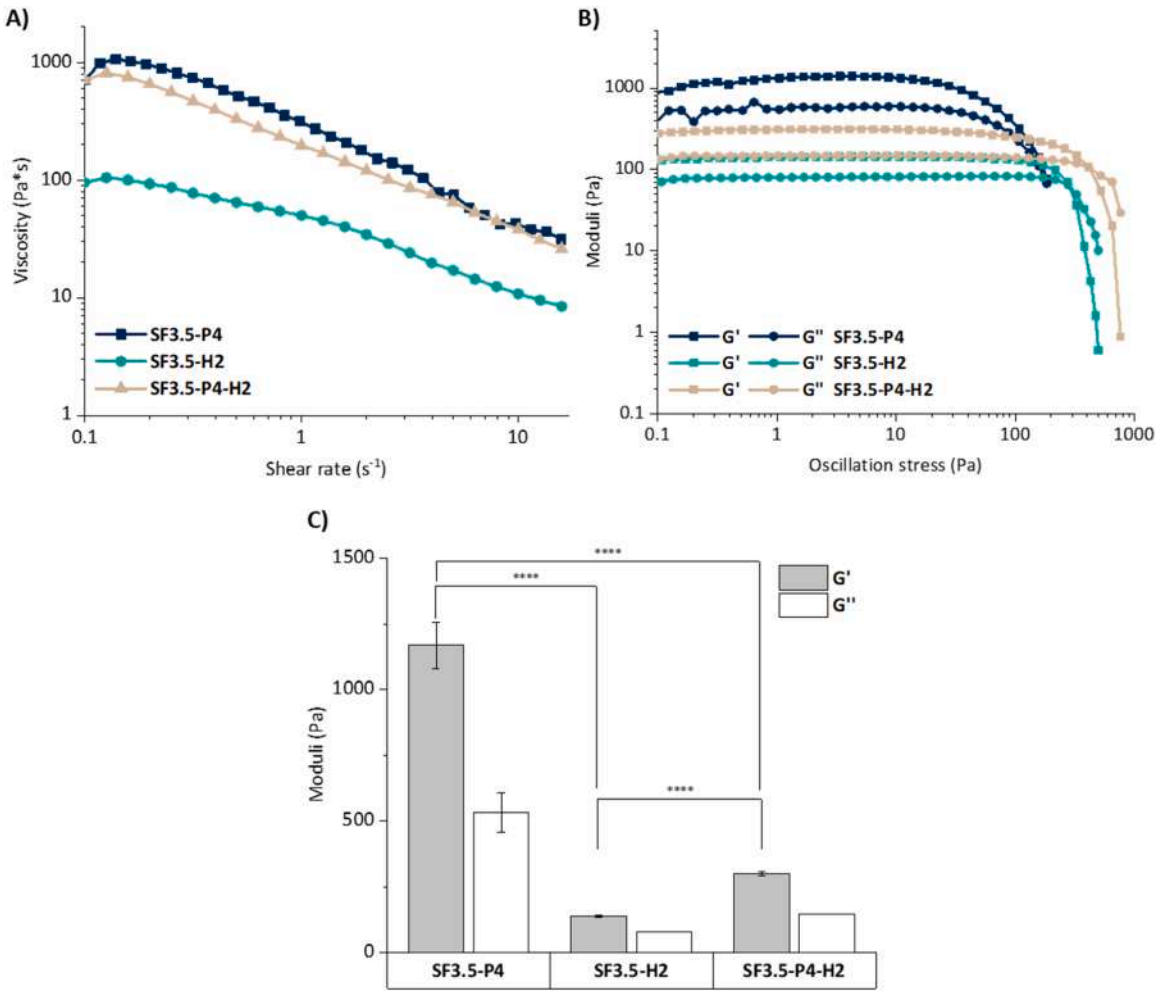

Fig. 10. Rheological testing of SF3.5-P4, SF3.5-P4-H2 and SF3.5-H2 hydrogels. A) Flow sweep curves, B) Oscillation stress curves and C) G' and G'' values (mean ± SD) in the LVER. **** $p \leq 0.0001$.

perturbation of the system (Figure S1) simulating the extrusion process in a timeframe of 240 s, with different G' values in accordance with oscillation tests. The behavior highlighted is an indicator of self-healing materials that can rapidly move from an elastic to a more viscous regime, requirement for a 3D printable material with improved printability and shape fidelity [7].

As the last step before printing, SF3.5-P4-H2 pre-gel was tested in its extrudability: a smooth, continuous and uniform filament was observed with a minimum extrusion pressure of 35 kPa, and no separation as previously reported for SF3.5-P4. Therefore, only the SF3.5-P4-H2 and SF3.5-H2 biomaterial inks were further tested to optimize printability (Fig. 11B).

The shape fidelity of SF3.5-P4-H2 ink was examined by means of the uniformity factor (UF) and the spreading ratio (SR) using standard image analysis methods, and compared to SF3.5-H2 herein used as control. Straight lines were printed at three different pressures (i.e., 35, 40 and 45 kPa) and three printing speeds (i.e., 5, 10, and 15 mm/s) to determine the optimal printing parameters (Figs. 11A and 11B).

Noticeably, and as expected, the SR of both SF3.5-P4-H2 and SF3.5-H2 increased while increasing the pressure and decreasing the velocity (Figs. 11A, 11B, 11E and 11F). This phenomenon is well reported in literature and attributed to the higher mass flow of material under these processing conditions. Moreover, excessive velocity during printing is reported to disrupt formation of a continuous filament while printing.

The UF values were all slightly higher than 1 but comparable in all the conditions, indicating a balanced crosslinking, which ensured a smooth extrusion (Figs. 11C and 11D) [63]. Notably, SR values were all in the range of 3–7 when using SF3.5-P4-H2 biomaterial ink (Fig. 11F), while higher values were reported in the case of SF3.5-H2 biomaterial ink (i.e., 4 – 11, Fig. 11E). This indicates and confirms that the use of P (i.e., UICP6 peptide) significantly enhances the printability (both rheological profile and shape fidelity) of the biomaterial ink and that the presence of HAMA counteracts any syneresis observed in SF-P pre-gels as initially hypothesized.

3.6. Physicochemical analysis on extruded hydrogels

Selected hydrogels (i.e., SF3.5-P4-H2 and SF3.5-H2) obtained after UV-crosslinking were tested in their stability in aqueous environment with a swelling test. For such tests, a 2% w/v HAMA hydrogel (H2) was used as a control. Fig. 12A showed a similar swelling profile of both the formulations SF3.5-P4-H2 and SF3.5-H2 for up to 21 days with slightly lower absolute values of the swelling ratio (range 35 – 65%), and comparable to the control H2 (range 70 – 80%). This was expected due to both the highly hydrophilic nature of HAMA, and the lower degree of crosslinking in H2 when compared to the blends [64]. We further investigated the inner morphology of SF3.5-P4-H2 and SF3.5-H2 (Fig. 12B) via FE-SEM. Both samples displayed a highly interconnected porous structure with mean diameters found to be in the range of 80–200 μm. Moreover, FT-IR was used to analyze the chemical composition of the samples and to evaluate their chemical composition and eventual changes in the secondary structure (Figure S2).

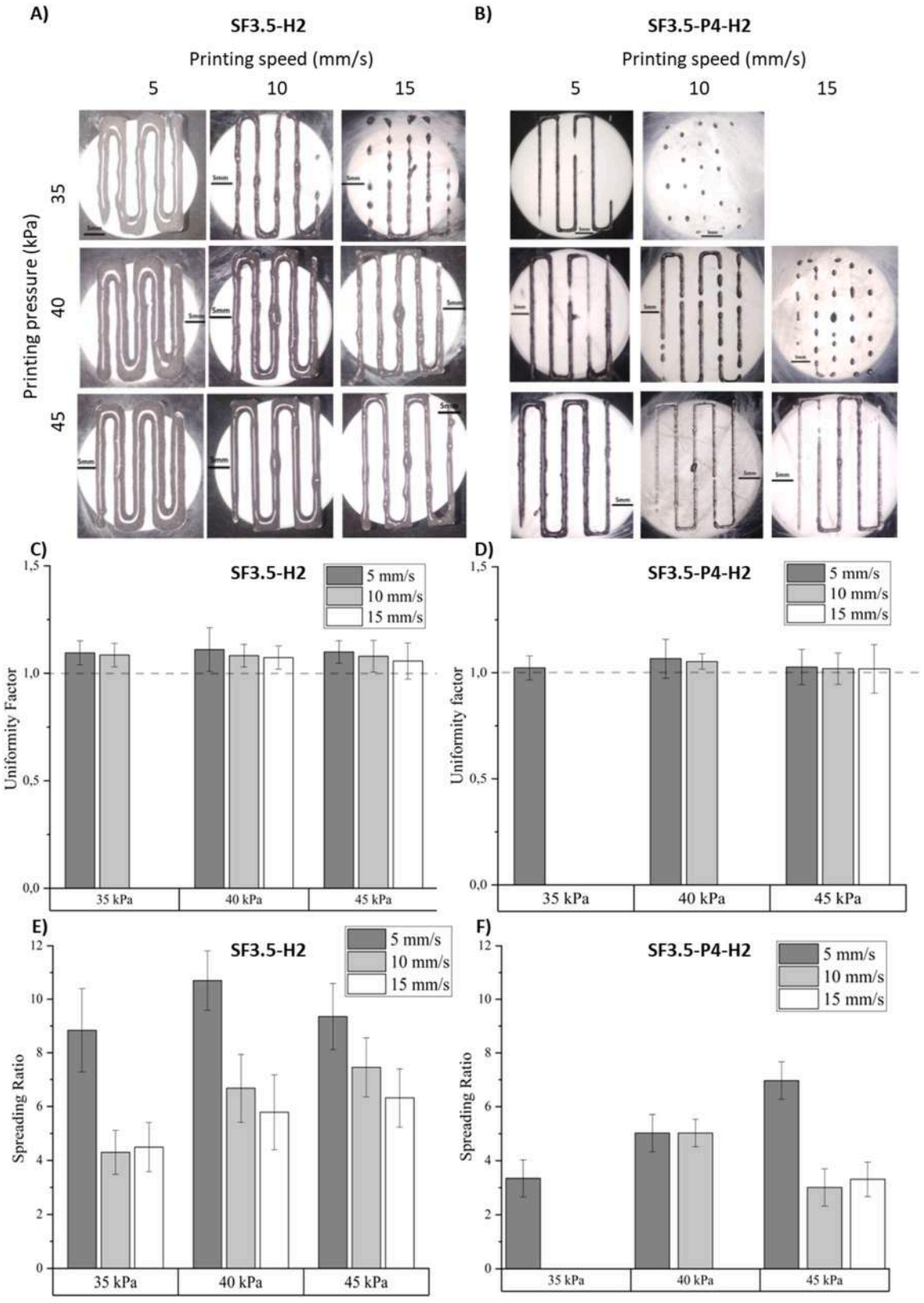

Fig. 11. Assessment of printability experiment. Printed straight lines varying pressure and speed of A) SF3.5-H2 and B) SF3.5-P4-H2. Analysis of the Uniformity Factor (UF) and Spreading Ratio (SR) of SF3.5-H2 (C,E) and SF3.5-P4-H2 (D,F) represented as (mean ± SD).

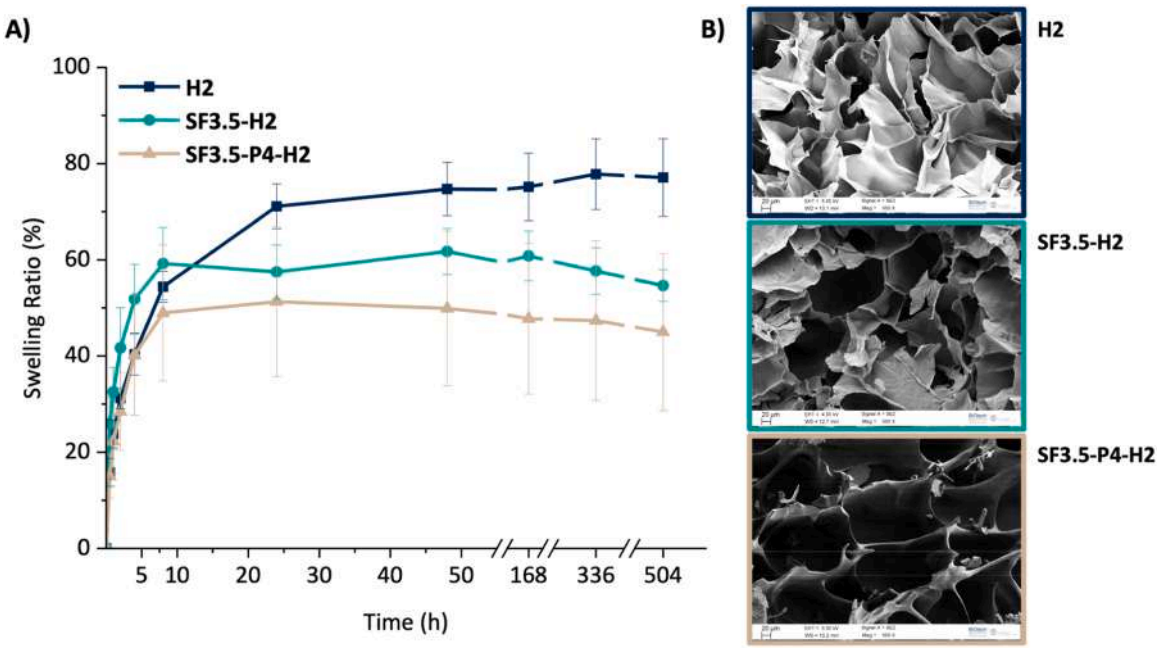

Fig. 12. A) Swelling ratio (mean ± SD) of SF3.5-H2, SF3.5-P4-H2 and H2. B) SEM images of SF3.5-H2, and SF3.5-P4-H2 and H2 (scale bar: 20 μm).

4. Conclusions

This study highlights the interaction of the *de novo* designed ultrashort self-assembling peptide UICP6 (P) and SF, as a proof-of-concept strategy for the use in extrusion-bioprinting (EBB). Results from the inverted vial test, ATR-FTIR, ThT binding fluorescence assay and SEM demonstrate that the inclusion of P triggers the hydrogelation of SF, forming a co-assembled hydrogel at or above a critical gelation concentration of P (3.0% w/v). In particular, higher concentrations of SF and P were associated with higher viscoelastic properties (G' and G'' values) and a modulation of the hydrogelation kinetics. Preliminary extrudability tests revealed that SF-P systems could not form continuous and homogeneous filaments due to syneresis. The incorporation of HAMA improved flow properties and printability by limiting syneresis effects, achieving better performance of the SF-P-HAMA when compared to the SF-HAMA biomaterial ink. Further, and most significantly, the inclusion of HAMA promotes a significant decrease of about 2.2-fold in the spreading ratio, proving the benefits of using a combination of P and SF in EBB for tissue engineering and regenerative medicine applications.

CRediT authorship contribution statement

Mohamed A. Elsawy: Writing – review & editing, Supervision, Resources, Project administration, Methodology, Funding acquisition, Data curation, Conceptualization. **Annalisa Tirella:** Writing – review & editing, Supervision, Resources, Project administration, Methodology, Funding acquisition, Data curation, Conceptualization. **Antonella Motta:** Writing – review & editing. **Devid Maniglio:** Writing – review & editing, Supervision, Resources. **Eugenia Spessot:** Writing – review & editing, Writing – original draft, Visualization, Validation, Resources, Methodology, Investigation, Formal analysis, Data curation, Conceptualization. **Abdulwahhab Khedr:** Writing – review & editing. **Gaia Pascolo:** Writing – review & editing, Visualization, Investigation, Data curation. **Soliman Mohamed A. N.:** Writing – review & editing, Visualization, Validation, Resources, Investigation, Formal analysis, Data curation. **Daniele Campoli:** Writing – review & editing, Writing – original draft, Visualization, Investigation, Formal analysis.

Funding

This project received fundings by the EU's Horizon 2020 Research and Innovation Programme under the Maria Sklodowska-Curie grant agreement no. 101008041 and by the Italian Ministry of Health under the funding program "Piano Sviluppo e Coesione Salute Traiettoria 4, Biotecnologie, Bioinformatica e Sviluppo Farmaceutico" through the project "LIFE4HUB - Living, Innovative, Fully Engineered, for Human Bioreplacement" (project code T4-CN-05).

Declaration of Competing Interest

The authors declare that they have no known competing financial interests or personal relationships that could have appeared to influence the work reported in this paper

Acknowledgments

This article is a revised and expanded version of a paper entitled A de novo designed ultrashort self-assembling peptide for the development of silk-based inks, which was presented at GNB2025, Palermo, June 16th-18th 2025 [59]. The authors would like to thank De Montfort University for hosting D.C. to perform FTIR measurements, as part of this project. E. S., A.M. and A.T. are grateful for the support of Fondazione VRT. M.E., M.A.N.S. and A.K. would like to thank The Egyptian Ministry of Higher Education & Scientific Research represented by The Egyptian Bureau for Cultural & Educational Affairs in London and The British Council for funding M.A.N.S. [MM22/19] and A.K. [NMM5/19] PhD work, which supported this project.

Appendix A. Supporting information

Supplementary data associated with this article can be found in the online version at doi:10.1016/j.nxmate.2026.102095.

References

[1] S. Naghieh, X. Chen, Printability–a key issue in extrusion-based bioprinting, J. Pharm. Anal. 11 (2021) 564–579, https://doi.org/10.1016/j.jpha.2021.02.001.

[2] N. Betancourt, X. Chen, Review of extrusion-based multi-material bioprinting processes, Bioprinting 25 (2022) e00189, https://doi.org/10.1016/j.bprint.2021.e00189.

[3] A.F. Bonatti, I. Chiesa, G. Vozzi, C. De Maria, Open-source CAD-CAM simulator of the extrusion-based bioprinting process, Bioprinting 24 (2021) e00172, https://doi.org/10.1016/j.bprint.2021.e00172.

[4] J.H.Y. Chung, S. Naficy, Z. Yue, R. Kapsa, A. Quigley, S.E. Moulton, G.G. Wallace, Bio-ink properties and printability for extrusion printing living cells, Biomater. Sci. 1 (2013) 763–773, https://doi.org/10.1039/C3BM00012E.

[5] T. Gao, G.J. Gillispie, J.S. Copus, A.K. PR, Y.-J. Seol, A. Atala, J.J. Yoo, S.J. Lee, Optimization of gelatin–alginate composite bioink printability using rheological parameters: a systematic approach, Biofabrication 10 (2018) 034106, https://doi.org/10.1088/1758-5090/aacdc7.

[6] D.A. Rau, M.J. Bortner, C.B. Williams, A rheology roadmap for evaluating the printability of material extrusion inks, Addit. Manuf. 75 (2023) 103745, https://doi.org/10.1016/j.addma.2023.103745.

[7] A. Schwab, R. Levato, M. D'Este, S. Piluso, D. Eglin, J. Malda, Printability and shape fidelity of bioinks in 3D bioprinting, Chem. Rev. 120 (2020) 11028–11055, https://doi.org/10.1021/acs.chemrev.0c00084.

[8] R.D. Abbott, E.P. Kimmerling, D.M. Cairns, D.L. Kaplan, Silk as a biomaterial to support long-term three-dimensional tissue cultures, ACS Appl. Mater. Interfaces 8 (2016) 21861–21868, https://doi.org/10.1021/acsami.5b12114.

[9] C. Holland, K. Numata, J. Rnjak-Kovacina, F.P. Seib, The biomedical use of silk: past, present, future, Adv. Healthc. Mater. 8 (2019) 1800465, https://doi.org/10.1002/adhm.201800465.

[10] D.N. Rockwood, R.C. Preda, T. Yücel, X. Wang, M.L. Lovett, D.L. Kaplan, Materials fabrication from Bombyx mori silk fibroin, Nat. Protoc. 6 (2011) 1612–1631, https://doi.org/10.1038/nprot.2011.379.

[11] T. Asakura, T. Tanaka, R. Tanaka, Advanced silk fibroin biomaterials and application to small-diameter silk vascular grafts, ACS Biomater. Sci. Eng. 5 (2019) 5561–5577, https://doi.org/10.1021/acsbiomaterials.8b01482.

[12] F. Agostinacchio, X. Mu, S. Dirè, A. Motta, D.L. Kaplan, Situ 3D printing: opportunities with silk inks, Trends Biotechnol. 39 (2021) 719–730, https://doi.org/10.1016/j.tibtech.2020.11.003.

[13] P.R. Laity, C. Holland, The rheology behind stress-induced solidification in native silk feedstocks, Int. J. Mol. Sci. 17 (2016) 1812, https://doi.org/10.3390/ijms17111812.

[14] T. Yucel, P. Cebe, D.L. Kaplan, Vortex-induced injectable silk fibroin hydrogels, Biophys. J. 97 (2009) 2044–2050, https://doi.org/10.1016/j.bpj.2009.07.028.

[15] A. Matsumoto, J. Chen, A.L. Collette, U.-J. Kim, G.H. Altman, P. Cebe, D.L. Kaplan, Mechanisms of silk fibroin sol−gel transitions, J. Phys. Chem. B 110 (2006) 21630–21638, https://doi.org/10.1021/jp056350v.

[16] O. Can Onder, S. Rubab Batool, M. Anwaar Nazeer, Self-assembled silk fibroin hydrogels: from preparation to biomedical applications, Mater. Adv. 3 (2022) 6920–6949, https://doi.org/10.1039/D2MA00568A.

[17] X. Mu, C. Gonzalez-Obeso, Z. Xia, J.K. Sahoo, G. Li, P. Cebe, Y.S. Zhang, D. L. Kaplan, 3D printing of monolithic proteinaceous cantilevers using regenerated silk fibroin, Molecules 27 (2022) 2148, https://doi.org/10.3390/molecules27072148.

[18] F. Agostinacchio, V. Fitzpatrick, S. Dirè, D.L. Kaplan, A. Motta, Silk fibroin-based inks for *in situ* 3D printing using a double crosslinking process, Bioact. Mater. 35 (2024) 122–134, https://doi.org/10.1016/j.bioactmat.2024.01.015.

[19] S. Sakai, T. Morita, One-step FRESH bioprinting of low-viscosity silk fibroin inks, ACS Biomater. Sci. Eng. 8 (2022) 2589–2597, https://doi.org/10.1021/acsbiomaterials.2c00269.

[20] C.A. Di Buduo, M. Lunghi, V. Kuzmenko, P.-A. Laurent, G. Della Rosa, C. Del Fante, D.E. Dalle Nogare, F. Jug, C. Perotti, K. Eto, A. Pecci, I.N. Redwan, A. Balduini, Bioprinting soft 3D models of hematopoiesis using natural silk fibroin-based Bioink efficiently supports platelet differentiation, Adv. Sci. 11 (2024) 2308276, https://doi.org/10.1002/advs.202308276.

[21] X. Du, D. Wei, L. Huang, M. Zhu, Y. Zhang, Y. Zhu, 3D printing of mesoporous bioactive glass/silk fibroin composite scaffolds for bone tissue engineering, Mater. Sci. Eng. C 103 (2019) 109731, https://doi.org/10.1016/j.msec.2019.05.016.

[22] S. Lipari, P. Sacco, E. Marsich, I. Donati, Silk fibroin-enriched bioink promotes cell proliferation in 3D-bioprinted constructs, Gels 10 (2024) 469, https://doi.org/10.3390/gels10070469.

[23] W. Shi, J. Zhang, Z. Gao, F. Hu, S. Kong, X. Hu, F. Zhao, Y. Ao, Z. Shao, Three-dimensional printed silk fibroin/hyaluronic acid scaffold with functionalized modification results in excellent mechanical strength and efficient endogenous cell recruitment for articular cartilage regeneration, Int. J. Mol. Sci. 25 (2024) 10523, https://doi.org/10.3390/ijms251910523.

[24] D. Trucco, A. Sharma, C. Manferdini, E. Gabusi, M. Petretta, G. Desando, L. Ricotti, J. Chakraborty, S. Ghosh, G. Lisignoli, Modeling and fabrication of silk fibroin–gelatin-based constructs using extrusion-based three-dimensional bioprinting, ACS Biomater. Sci. Eng. 7 (2021) 3306–3320, https://doi.org/10.1021/acsbiomaterials.1c00410.

[25] J. Yang, Z. Li, S. Li, Q. Zhang, X. Zhou, C. He, Tunable metacrylated silk fibroin-based hybrid bioinks for the bioprinting of tissue engineering scaffolds, Biomater. Sci. 11 (2023) 1895–1909, https://doi.org/10.1039/D2BM01978G.

[26] Y.-C. Yeh, P.-Y. Chen, K.-T. Chen, I.-C. Lee, Innovative MXene/SilMA-based conductive bioink for three dimensional bioprinting of neural stem cell spheroids in neural tissue engineering, ACS Appl. Mater. Interfaces 17 (2025) 10402–10416, https://doi.org/10.1021/acsami.4c19373.

[27] A. Khedr, M.A.N. Soliman, M.A. Elsawy, Design rules for self-assembling peptide nanostructures, in: M.A. Elsawy (Ed.), Peptide Bionanomaterials: From Design to Application, Springer International Publishing, Cham, 2023, pp. 1–52, https://doi.org/10.1007/978-3-031-29360-3_1.

[28] E.H. Field, J. Ratcliffe, C.J. Johnson, K.J. Binger, N.P. Reynolds, Self-healing, 3D printed bioinks from self-assembled peptide and alginate hybrid hydrogels, Biomater. Adv. 169 (2025) 214145, https://doi.org/10.1016/j.bioadv.2024.214145.

[29] D.M. Alhattab, Z. Khan, S. Alshehri, H.H. Susapto1, C.A.E. Hauser, 3D bioprinting of ultrashort self-assembling peptides to engineer scaffolds with different matrix stiffness for chondrogenesis, Int. J. Bioprint 9 (2023) 719, https://doi.org/10.18063/ijb.719.

[30] M.A.N. Soliman, A. Khedr, T. Sahota, R. Armitage, R. Allan, K. Laird, N. Allcock, F. I. Ghuloum, M.H. Amer, R. Alazragi, C.J.C. Edwards-Gayle, J.K. Wychowaniec, A. V. Vargiu, M.A. Elsawy, Unraveling the atomistic mechanism of electrostatic lateral association of peptide β-sheet structures and its role in nanofiber growth and hydrogelation, Small (2025) 2408213, https://doi.org/10.1002/smll.202408213.

[31] J.K. Wychowaniec, R. Patel, J. Leach, R. Mathomes, V. Chhabria, Y. Patil-Sen, A. Hidalgo-Bastida, R.T. Forbes, J.M. Hayes, M.A. Elsawy, Aromatic stacking facilitated self-assembly of ultrashort ionic complementary peptide sequence: β-sheet nanofibers with remarkable gelation and interfacial properties, Biomacromolecules 21 (2020) 2670–2680, https://doi.org/10.1021/acs.biomac.0c00366.

[32] B. Cheng, Y. Yan, J. Qi, L. Deng, Z.-W. Shao, K.-Q. Zhang, B. Li, Z. Sun, X. Li, Cooperative assembly of a peptide gelator and silk fibroin afford an injectable hydrogel for tissue engineering, ACS Appl. Mater. Interfaces 10 (2018) 12474–12484, https://doi.org/10.1021/acsami.8b01725.

[33] F. Feng, X. Song, Z. Tan, Y. Tu, L. Xiao, P. Xie, Y. Ma, X. Sun, J. Ma, L. Rong, L. He, Cooperative assembly of a designer peptide and silk fibroin into hybrid nanofiber gels for neural regeneration after spinal cord injury, Sci. Adv. 9 (2023) eadg0234, https://doi.org/10.1126/sciadv.adg0234.

[34] Y. Loo, A. Lakshmanan, M. Ni, L.L. Toh, S. Wang, C.A.E. Hauser, Peptide bioink: self-assembling nanofibrous scaffolds for three-dimensional organotypic cultures, Nano Lett. 15 (2015) 6919–6925, https://doi.org/10.1021/acs.nanolett.5b02859.

[35] C. Cofiño, S. Perez-Amodio, C.E. Semino, E. Engel, M.A. Mateos-Timoneda, Development of a self-assembled peptide/methylcellulose-based bioink for 3D bioprinting, Macromol. Mater. Eng. 304 (2019) 1900353, https://doi.org/10.1002/mame.201900353.

[36] C. Loebel, C.B. Rodell, M.H. Chen, J.A. Burdick, Shear-thinning and self-healing hydrogels as injectable therapeutics and for 3D-printing, Nat. Protoc. 12 (2017) 1521–1541, https://doi.org/10.1038/nprot.2017.053.

[37] S.A. Hudson, H. Ecroyd, T.W. Kee, J.A. Carver, The thioflavin T fluorescence assay for amyloid fibril detection can be biased by the presence of exogenous compounds, FEBS J. 276 (2009) 5960–5972, https://doi.org/10.1111/j.1742-4658.2009.07307.x.

[38] F. Perin, E. Spessot, A. Famà, A. Bucciarelli, E. Callone, C. Mota, A. Motta, D. Maniglio, Modeling a dynamic printability window on polysaccharide blend inks for extrusion bioprinting, ACS Biomater. Sci. Eng. 9 (2023) 1320–1331, https://doi.org/10.1021/acsbiomaterials.2c01143.

[39] E. Spessot, S. Passuello, L.V. Shah, D. Maniglio, A. Motta, Nanocomposite methacrylated silk fibroin-based scaffolds for bone tissue engineering, Biomimetics 9 (2024) 218, https://doi.org/10.3390/biomimetics9040218.

[40] A. Khedr, M.A.N. Soliman, A. Corrigan, T. Sahota, R. Armitage, N. Allcock, J. T. Jegadeesan, M.H. Amer, R. Alazragi, Z. Ahmad, J.K. Wychowaniec, M.A. Elsawy, Charge directed selective co-assembly of ionic complementary peptide binary mixtures, Small 22 (2026) e13140, https://doi.org/10.1002/smll.202513140.

[41] X. Wu, J. Hou, M. Li, J. Wang, D.L. Kaplan, S. Lu, Sodium dodecyl sulfate-induced rapid gelation of silk fibroin, Acta Biomater. 8 (2012) 2185–2192, https://doi.org/10.1016/j.actbio.2012.03.007.

[42] D. Chouhan, T. Lohe, P.K. Samudrala, B.B. Mandal, Situ forming injectable silk fibroin hydrogel promotes skin regeneration in full thickness burn wounds, Adv. Healthc. Mater. 7 (2018) 1801092, https://doi.org/10.1002/adhm.201801092.

[43] G.W. Scherer, Mechanics of syneresis I. Theory, J. Non-Cryst. Solids 108 (1989) 18–27, https://doi.org/10.1016/0022-3093(89)90328-1.

[44] R. Yadav, R. Purwar, Influence of metal oxide nanoparticles on morphological, structural, rheological and conductive properties of mulberry silk fibroin nanocomposite solutions, Polym. Test. 93 (2021) 106916, https://doi.org/10.1016/j.polymertesting.2020.106916.

[45] M. Boulet-Audet, F. Vollrath, C. Holland, Identification and classification of silks using infrared spectroscopy, J. Exp. Biol. 218 31383149 (2015), https://doi.org/10.1242/jeb.128306.

[46] F. Mukasheva, L. Adilova, A. Dyussenbinov, B. Yernaimanova, M. Abilev, D. Akilbekova, Optimizing scaffold pore size for tissue engineering: insights across various tissue types, Front. Bioeng. Biotechnol. 12 (2024), https://doi.org/10.3389/fbioe.2024.1444986.

[47] Q. Lu, H. Zhu, C. Zhang, F. Zhang, B. Zhang, D.L. Kaplan, Silk self-assembly mechanisms and control from thermodynamics to kinetics, Biomacromolecules 13 (2012) 826–832, https://doi.org/10.1021/bm201731e.

[48] A. Kamada, Z. Toprakcioglu, T.P.J. Knowles, Kinetic ANalysis Reveals the Role of Secondary Nucleation in Regenerated Silk Fibroin Self-assembly, Biomacromolecules 24 (2023) 1709–1716, https://doi.org/10.1021/acs.biomac.2c01479.

[49] A. Matsumoto, J. Chen, A.L. Collette, U.-J. Kim, G.H. Altman, P. Cebe, D.L. Kaplan, Mechanisms of silk fibroin sol−gel transitions, J. Phys. Chem. B 110 (2006) 21630–21638, https://doi.org/10.1021/jp056350v.

[50] C. Wu, Y. Duan, L. Yu, Y. Hu, C. Zhao, C. Ji, X. Guo, S. Zhang, X. Dai, P. Ma, Q. Wang, S. Ling, X. Yang, Q. Dai, In-situ observation of silk nanofibril assembly via

graphene plasmonic infrared sensor, Nat. Commun. 15 (2024) 4643, https://doi.org/10.1038/s41467-024-49076-5.
[51] Z. Chen, H. Zhang, Z. Lin, Y. Lin, J.H. van Esch, X.Y. Liu, Programing performance of silk fibroin materials by controlled nucleation, Adv. Funct. Mater. 26 (2016) 8978–8990, https://doi.org/10.1002/adfm.201602908.
[52] K. Hölzl, S. Lin, L. Tytgat, S.V. Vlierberghe, L. Gu, A. Ovsianikov, Bioink properties before, during and after 3D bioprinting, Biofabrication 8 (2016) 032002, https://doi.org/10.1088/1758-5090/8/3/032002.
[53] S. Boularaoui, G. Al Hussein, K.A. Khan, N. Christoforou, C. Stefanini, An overview of extrusion-based bioprinting with a focus on induced shear stress and its effect on cell viability, Bioprinting 20 (2020) e00093, https://doi.org/10.1016/j.bprint.2020.e00093.
[54] E.J. Hemingway, S.M. Fielding, Edge fracture instability in sheared complex fluids: onset criterion and possible mitigation strategy, J. Rheol. 63 (2019) 735–750, https://doi.org/10.1122/1.5095717.
[55] E.J. Hemingway, H. Kusumaatmaja, S.M. Fielding, Edge fracture in complex fluids, Phys. Rev. Lett. 119 (2017) 028006, https://doi.org/10.1103/PhysRevLett.119.028006.
[56] G. Gillispie, P. Prim, J. Copus, J. Fisher, A.G. Mikos, J.J. Yoo, A. Atala, S.J. Lee, Assessment methodologies for extrusion-based bioink printability, Biofabrication 12 (2020) 022003, https://doi.org/10.1088/1758-5090/ab6f0d.
[57] D. Petta, U. D'Amora, L. Ambrosio, D.W. Grijpma, D. Eglin, M. D'Este, Hyaluronic acid as a bioink for extrusion-based 3D printing, Biofabrication 12 (2020) 032001, https://doi.org/10.1088/1758-5090/ab8752.
[58] D. Petta, D.W. Grijpma, M. Alini, D. Eglin, M. D'Este, Three-dimensional printing of a tyramine hyaluronan derivative with double gelation mechanism for independent tuning of shear thinning and postprinting curing, ACS Biomater. Sci. Eng. 4 (2018) 3088–3098, https://doi.org/10.1021/acsbiomaterials.8b00416.
[59] E. Spessot, X. Bai, D. Moranduzzo, C. Zhao, S. Butterworth, D. Maniglio, A. Tirella, Exploiting nano-in-micro-technologies to couple PLGA-hydroxyl-FK866 nanoparticles to a hydrogel network for local drug release, RSC Pharm. 2 (2025) 718–730, https://doi.org/10.1039/D4PM00334A.
[60] Faers, M.A., Choudhury, T.H., Lau, B., McAllister, K., Luckham, P.F., 2006. Syneresis and rheology of weak colloidal particle gels. Colloids and Surfaces A: Physicochemical and Engineering Aspects, Papers from "Formula IV: Frontiers in Formulation Science", an International conference organised by the RSC, held in London, July 4-7th 2005 288, 170–179. https://doi.org/10.1016/j.colsurfa.2006.03.031.
[61] Q. Wu, J. Buijs, S. de Groot, H.M. van der Kooij, J. van der Gucht, T.E. Kodger, Spatially heterogenous dynamics in colloidal gels during syneresis, Soft Matter 19 (2023) 5336–5344, https://doi.org/10.1039/D3SM00448A.
[62] G.G.G. Perera, D.F. Argenta, T. Caon, The rheology of injectable hyaluronic acid hydrogels used as facial fillers: a review, Int. J. Biol. Macromol. 268 (2024) 131880, https://doi.org/10.1016/j.ijbiomac.2024.131880.
[63] C. O'Connell, J. Ren, L. Pope, Y. Li, A. Mohandas, R. Blanchard, S. Duchi, C. Onofrillo, Characterizing bioinks for extrusion bioprinting: printability and rheology, in: J.M. Crook (Ed.), 3D Bioprinting: Principles and Protocols, Methods in Molecular Biology, Springer US, New York, NY, 2020, pp. 111–133, https://doi.org/10.1007/978-1-0716-0520-2_7.
[64] M. Mahkam, L. Doostie, The relation between swelling properties and cross-linking of hydrogels designed for colon-specific drug delivery, Drug Deliv. 12 (2005) 343–347, https://doi.org/10.1080/10717540590952627.